Sub-THz signals' propagation model in hypersonic plasma sheath under different atmospheric conditions

Kai YUAN[1], Yuhao WANG[2], Linfang SHEN[1], Ming YAO[1],
Xiaohua DENG[1*], Fuhui ZHOU[2] & Zhou CHEN[1]

[1]*Institute of Space Science and Technology, Nanchang University, Nanchang 330031, China;*
[2]*Information Engineering School, Nanchang University, Nanchang 330031, China*

Abstract One of the aims for modern hypersonic cruise flight is hypersonic global reach. The length of route for such flights could be up to thousands of kilometers. The atmospheric conditions on the route are complicated. On the other hand, hypersonic flights used to suffer from communication blackout. The sub-THz communication is considered as a potential solution to the 'blackout'. In the present study the propagation for sub-THz signals in hypersonic plasma sheaths was modeled under different atmospheric conditions. According to the study, the electron density and the electron collision frequency near the onboard antenna linearly increase with the atmospheric mass density around the vehicle, hence the attenuation of sub-THz signals in hypersonic plasma sheaths increases with the atmospheric mass density. The impact led by the atmospheric temperature is ignorable. Based on the study a new sub-THz signals' propagation model was developed, which could be utilized for quick estimation for signal propagation under different atmospheric conditions. The geographical difference of signal propagation over the whole globe was obtained with the new model. The results showed that the signal attenuation in plasma sheaths varies with latitude and longitude. The maximum signal attenuation occurs in Alaska, Canada and Russia.

Keywords sub-THz communication, hypersonic cruise flight, communication blackout, plasma sheath, signal propagation model, signal attenuation

1 Introduction

Modern hypersonic vehicles, which include reentry capsules, ballistic missiles and hypersonic cruise flights, used to suffer from communication blackout in near space [1]. Although scientists and engineers have made great efforts to solve the problem, the 'blackout' is still a challenge to modern aero and space engineering so far. On the other hand, the hypersonic cruise flight, which aims at hypersonic global reach, is being concerned by many countries nowadays. The communication blackout is an obstacle for the implementation of such flights. The sub-THz communication is considered as a potential solution to the blackout problem. The sub-THz band covers the frequencies in the range from 50 GHz to 1 THz [2,3], which is normally higher than the maximum cutoff frequency in hypersonic plasma sheaths.

---

* Corresponding author (email: deng_x_h@163.com)

According to previous theoretical and experimental studies, carrier waves in sub-THz band could penetrate dense plasma slab [4,5]. Scientists have started to design the sub-THz communication system to solve the communication blackout problem [6]. On the other hand, the dense plasma is a very severe and complicated environment for signal propagation. The attenuation of sub-THz signals in dense plasma slab are impacted by the inhomogeneity of the plasma [7], the electron density, the electron collision frequency, the temperature, and the thickness of the plasma slab [8]. The communication blackout would occur if the signals that reach the antenna is too weak to be detected. Moreover, the propagation of sub-THz signals in realistic hypersonic plasma sheaths could be different from that in presumed plasma slabs since all the parameters of a hypersonic plasma sheath vary simultaneously [9]. It implies that the propagation of sub-THz signals in hypersonic plasma sheaths could be much more complicated than that in plasma slabs. In other words, the hypersonic plasma sheath, which is nonuniform media for signal propagation, must be paid attention to in order to solve the problem of communication blackout.

Previous studies have revealed that the hypersonic plasma sheath is influenced by many factors including the aerodynamic shape [10], the angle of attack [11, 12] and the flight trajectory [13]. Besides those parameters, the plasma sheath is obviously influenced by the atmospheric conditions around the hypersonic vehicle. Hence the signal propagation in plasma sheaths is influenced by the atmospheric conditions as the results. On the other hand, the length of route for a hypersonic cruise flight could be up to thousands of kilometers. It could be expected that the signal propagation in the plasma sheath varies with the location of flight due to the geographical difference of atmospheric conditions.

In the present study, the sub-THz signal propagation in hypersonic plasma sheaths under different atmospheric conditions was studied. The hypersonic plasma sheaths under different atmospheric conditions were obtained with a numerical hypersonic fluid model. The relation between the signal propagation and the atmospheric conditions was analyzed accordingly. Based on the numerical study and the analysis, a new estimation model was developed, which could be utilized for quick estimation of sub-THz signal propagation in hypersonic plasma sheath under different atmospheric conditions. The results obtained with the quick estimation model agree well with the results obtained based on the hypersonic fluid model. The global distribution of sub-THz signal attenuation in hypersonic plasma sheath was obtained with the new model. The geographical difference of the signal attenuation was revealed accordingly.

2 Hypersonic fluid model

The hypersonic plasma sheath is the nonuniform media for signal propagation. In the present study the plasma sheath was modeled with the conservative form of Navier-Stokes (N-S) equations and the gas molecular theories [9, 14]. Eqs. (1)–(3) are the N-S equations:

$$\frac{\partial \rho}{\partial t} + \nabla \cdot (\rho \vec{u}) = 0, \tag{1}$$

$$\frac{\partial (\rho \vec{u})}{\partial t} + \nabla \cdot \left(\rho \vec{u} \otimes \vec{u} + p \vec{\vec{I}} \right) = \nabla \cdot \vec{\vec{\tau}}, \tag{2}$$

$$\frac{\partial e}{\partial t} + \nabla \cdot [\vec{u}(e + p)] = \nabla \cdot \left(\vec{\vec{\tau}} \cdot \vec{u} \right) + \nabla \cdot (k_{\text{T}} \nabla T), \tag{3}$$

where $\vec{u}$, ρ, p, e, k_{T}, T, $\vec{\vec{I}}$ and $\vec{\vec{\tau}}$ are fluid velocity, mass density, pressure, total energy, thermal conductivity, temperature, unit tensor and viscous stress tensor, respectively. The mass density, pressure, viscous stress tensor and the total energy are expressed as

$$\rho = \sum_i^N n_i m_i, \tag{4}$$

$$p = \rho R T, \tag{5}$$

$$\vec{\vec{\tau}} = -\frac{2}{3} \mu \left(\nabla \cdot \vec{u} \right) \vec{\vec{I}} + \mu \left[\nabla \otimes \vec{u} + (\nabla \otimes \vec{u})^{\text{T}} \right], \tag{6}$$

$$e = \frac{p}{\gamma - 1} + \frac{1}{2}\rho\vec{u} \cdot \vec{u} + \sum_i^N n_i H_i, \tag{7}$$

where μ is the dynamic viscosity, H is the enthalpy of formation, γ is the ratio between the specific heat at constant pressure and the specific heat at constant volume. The superscript T in (6) is the transpose operator.

The number density continuity equation is introduced in order to close the system of equations for the present model.

$$\frac{\partial n_i}{\partial t} + \nabla \cdot (n_i \vec{u}) = s_i, \tag{8}$$

where s_i is the source term for the i-th species led by chemical reactions.

The rest of necessary variables are obtained from gas kinetic theories [15]:

$$\mu_i = \frac{5}{16} \frac{\sqrt{\pi m_i k_B T}}{\pi \sigma^2 \Omega}, \tag{9}$$

$$c_{Pi} = \left(\frac{f}{2} + 1\right) R_i, \tag{10}$$

$$c_{Vi} = c_{Pi} - R_i, \tag{11}$$

$$k_{Ti} = \frac{5}{2} c_{Vi} \mu_i, \tag{12}$$

where σ is the collision diameter, Ω is the collision integral, k_B is the Boltzmann constant, f is the degree of freedom, R is the gas constant, c_P and c_V are the specific heat of constant pressure and the specific heat of constant volume, respectively.

The chemical reactions are modeled with the air 7-species model. The altitude of the flight is fixed to be 30 km in the present study since the severest communication blackout occurred at the same altitude in the RAMC-II (Radio Attenuation Measurements C-II) reentry experiment. The flight speed is 6550 m/s, which is identical to the RAMC-II vehicle at the same altitude. The atmospheric conditions were obtained from MSIS-E-90 atmospheric model.

3 Results and analysis

3.1 The hypersonic plasma sheath

The hypersonic plasma sheath was modeled under different atmospheric conditions, which are listed in Table 1. The sub-THz signal attenuation in a realistic hypersonic plasma sheath is determined by the electron density and the electron collision frequency [9]. Figure 1 shows the electron density and the electron collision frequency distributions for the hypersonic plasma sheath at equator, which is one of the 11 cases simulated in the present study.

The onboard antenna is assumed to be on the wall of the vehicle, which is 1.05 m away from the nose cap. The 'atmospheric window' frequencies, which are 94, 140 and 225 GHz [16], are concerned in the present study. The incident angle for the carrier waves are assumed to be 0°. The dashed line in Figure 1(a) denotes the propagation path for the signals towards the onboard antenna. The electron collision frequency illustrated in Figure 1(b) was calculated according to [17]

$$f_{en} = 3 \times 10^8 \left(\frac{\rho}{\rho_0}\right) T, \tag{13}$$

where $\rho_0 = 1.28823$ kg/m^3.

Figure 2 illustrates the plasma parameters near the antenna against the atmospheric conditions. According to Figure 2, the hypersonic plasma sheath varies with atmospheric conditions. Generally all the parameters showed in Figure 2 increase with the atmospheric mass density (ρ_A). However, those parameters do not have clear relations with the atmospheric temperature (T_A). The reason is that the T_A is

Table 1 The atmospheric conditions

|	Latitude	Longitude	Mass density (kg/m^3)	Temperature (K)
1	90°S	50°E	8.701×10^{-3}	224.5
2	45°N	50°E	1.682×10^{-2}	232.5
3	68°S	50°E	1.011×10^{-2}	230.4
4	50°S	50°E	1.321×10^{-2}	231.3
5	0°	50°E	1.566×10^{-2}	230.9
6	68°N	50°E	1.659×10^{-2}	234.7
7	45°S	50°E	1.402×10^{-2}	231.3
8	15°S	50°E	1.567×10^{-2}	231.2
9	15°N	50°E	1.606×10^{-2}	231.0
10	30°S	50°E	1.550×10^{-2}	231.3
11	30°N	50°E	1.658×10^{-2}	231.5
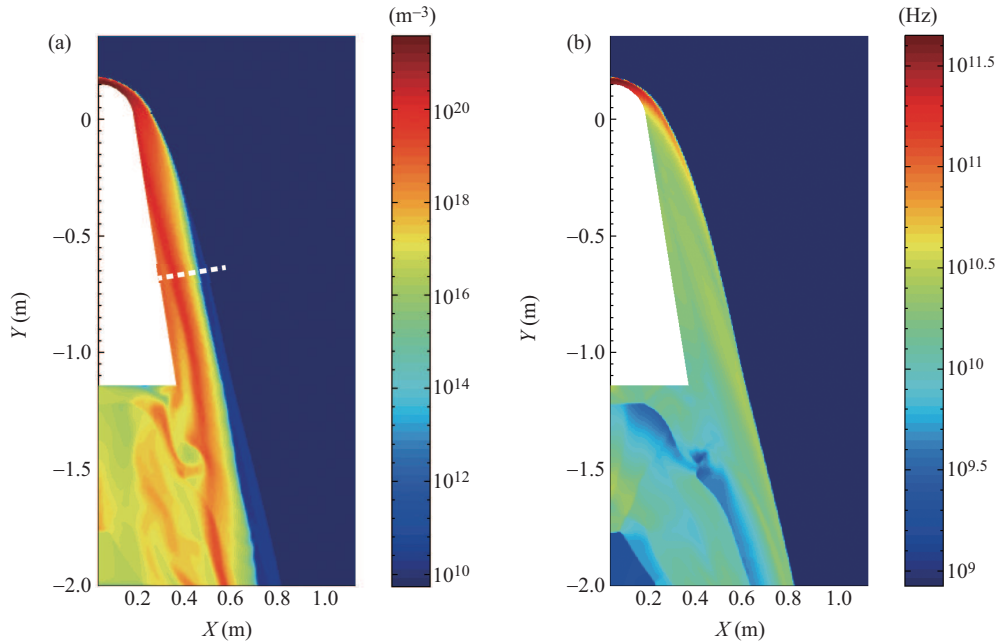
Figure 1 (Color online) The electron density (a) and the electron collision frequency (b) of the plasma sheath (at equator).

in the range from about 225 to 235 K. The difference between the maximum and the minimum is only 10 K, which is ignorable compared with the temperature itself. On the other hand, the minimum and the maximum ρ_A are about 0.009 and 0.017 kg/m^3, respectively. The maximum is almost two times of the minimum. In such a case the variation of the atmospheric mass density makes more significant impacts on the plasma sheath in practice. Additionally, it should be noticed that both the maxima electron density and the maxima electron collision frequency seem to have linear relations with the atmospheric mass density (see Figure 2(b)). Figure 3 shows more detail about the linear relations.
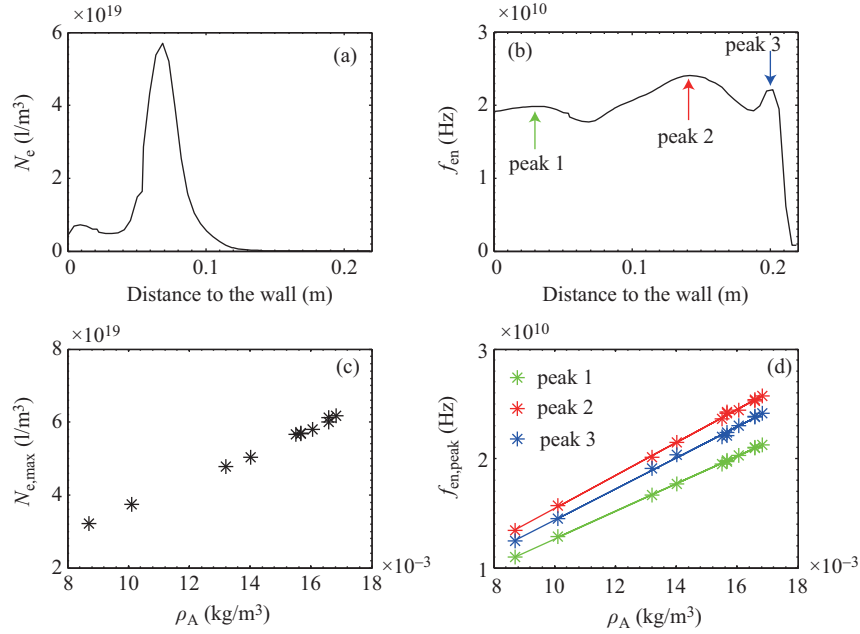
The profiles for the electron density and the electron collision frequency along the signal propagation path are illustrated in Figure 3(a) and (b), respectively. Note that there are three peaks on the profile of electron collision frequency. Interestingly, the maximum electron density and the three peaks of electron collision frequency have positive linear relations with the atmospheric mass density (see Figure 3(c) and (d)).

3.2 The propagation of sub-THz signals

The wavelengths corresponding to the concerned frequencies are much smaller than the spatial scale of the inhomogeneity of the plasma sheath. In such a case, the plasma along the signal propagation path
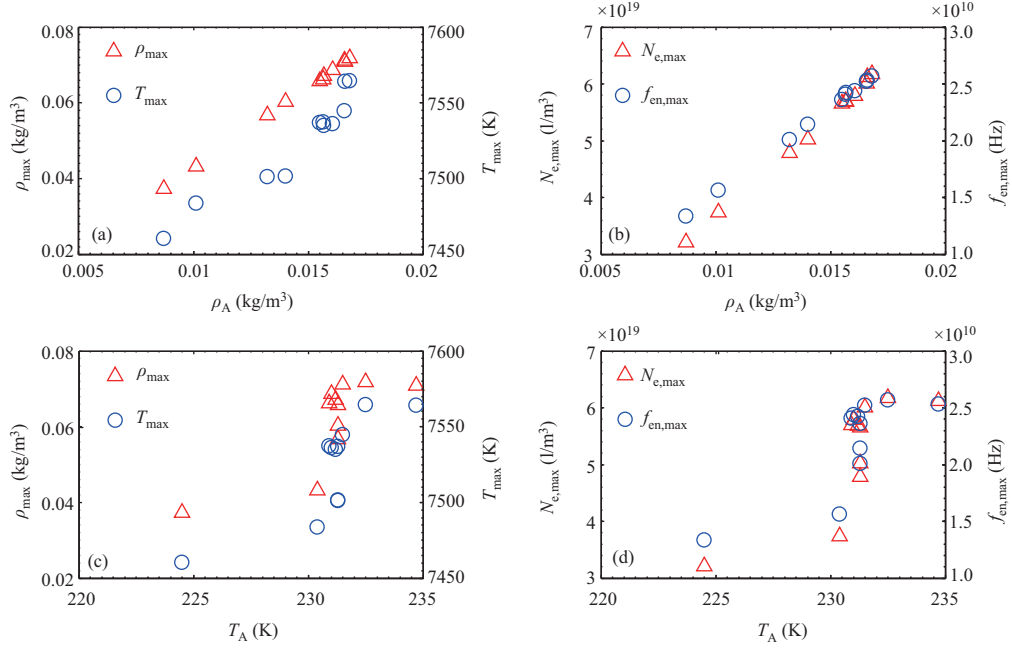
Figure 2 (Color online) The maxima of plasma parameters near the antenna vs. the atmospheric conditions. (a) Maxima of mass density and the temperature vs. atmospheric mass density; (b) maxima of electron density and collision frequency vs. atmospheric mass density; (c) maxima of mass density and temperature vs. atmospheric temperature; (d) maxima electron density and collision frequency vs. atmospheric temperature.

Figure 3 (Color online) (a) The electron density profile, (b) electron collision frequency profile, (c) maximum electron density against the atmospheric mass density and (d) the peak values for the electron collision frequency against the atmospheric mass density.

could be treated as a one dimensional plasma slab. The slab was divided into several layers, and the plasma parameters in each layer are considered to be homogeneous.

The maximum electron density on the propagation path of sub-THz signals is smaller than 6×10^{19} /m^3 (see Figure 3(a)), i.e., the maximum cutoff frequency is about 69 GHz, which is much lower than 94 GHz. In such a case the reflections are ignorable. The attenuation is the main mechanism

of energy loss for signal propagations. The incident angle in the present study is always 0°, then the polarization loss for the signals is ignorable. In a homogeneous plasma slab, the propagation constant for the electromagnetic (EM) waves is expressed as [1]

$$\gamma_{\mathrm{p}} = \alpha_{\mathrm{p}} - \mathrm{j}\beta_{\mathrm{p}}. \tag{14}$$

In the inhomogeneous plasma slab, the expression becomes

$$\gamma_{\mathrm{p}}(l) = \alpha_{\mathrm{p}}(l) - \mathrm{j}\beta_{\mathrm{p}}(l), \tag{15}$$

where l is the distance to the antenna, α_{p} is the attenuation coefficient and β_{p} is the phase coefficient.

$$\alpha_{\mathrm{p}}(l) = k_0 \sqrt{\left\{ \left[K_r(l)^2 + K_i(l)^2 \right]^{1/2} - K_r(l) \right\} \Big/ 2}, \tag{16}$$

$$\beta_{\mathrm{p}}(l) = k_0 \sqrt{\left\{ \left[K_r(l)^2 + K_i(l)^2 \right]^{1/2} + K_r(l) \right\} \Big/ 2}, \tag{17}$$

with

$$K_r(l) = 1 - \frac{\omega_{\mathrm{p}}(l)^2}{\omega^2 + \nu(l)^2}, \tag{18}$$

$$K_i(l) = \frac{\omega_{\mathrm{p}}(l)^2 \left[\nu(l)/\omega \right]}{\omega^2 + \nu(l)^2}, \tag{19}$$

$$\omega_{\mathrm{p}}(l) = \sqrt{\frac{eN_{\mathrm{e}}(l)}{m_{\mathrm{e}}\varepsilon_0}}, \tag{20}$$

$$\nu(l) = 2\pi f_{\mathrm{en}}(l). \tag{21}$$

The total signal attenuation is defined as

$$\mathrm{Att} = \frac{|E_0|^2}{|E_{\mathrm{t}}|^2} = \left| \exp\left[\int_0^L 2\gamma_{\mathrm{p}}(l)\,\mathrm{d}l \right] \right|, \tag{22}$$

where L is the length of the transmission path, E_{t} is the electric field for the transmitted wave, and E_0 is the electric field for the incident wave. The total signal attenuation (Att) under different atmospheric conditions are illustrated in Figure 4.

According to Figure 4(a), the Att for the concerned frequencies increases with the atmospheric mass density. For the identical mass densities, the Att increases with the frequency. On the other hand, Figure 4(b) showed that there is not any clear relation between the Att and the atmospheric temperature. It indicates that the atmospheric mass density makes more significant impact on both the hypersonic plasma sheath and the total signal attenuation.

3.3 The character of energy loss for sub-THz signals

Obviously the total signal attenuation in hypersonic plasma sheath is determined by the attenuation coefficient α, which varies with the distance to the antenna. Figure 5 illustrates the profiles for the attenuation coefficients along the signal propagation path. Also the profiles for the electron density and the electron collision frequency are illustrated in Figure 5(a) and (b), respectively. Figure 5 shows that the signal attenuation mainly occurs in the area where the electrons concentrate.
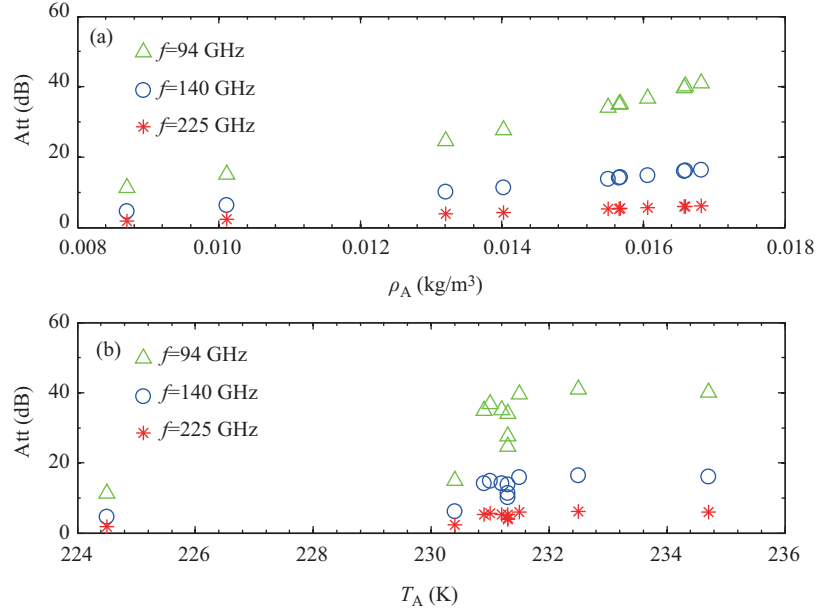
Figure 4   (Color online) The total signal attenuation vs. (a) atmospheric mass density and (b) atmospheric temperature.
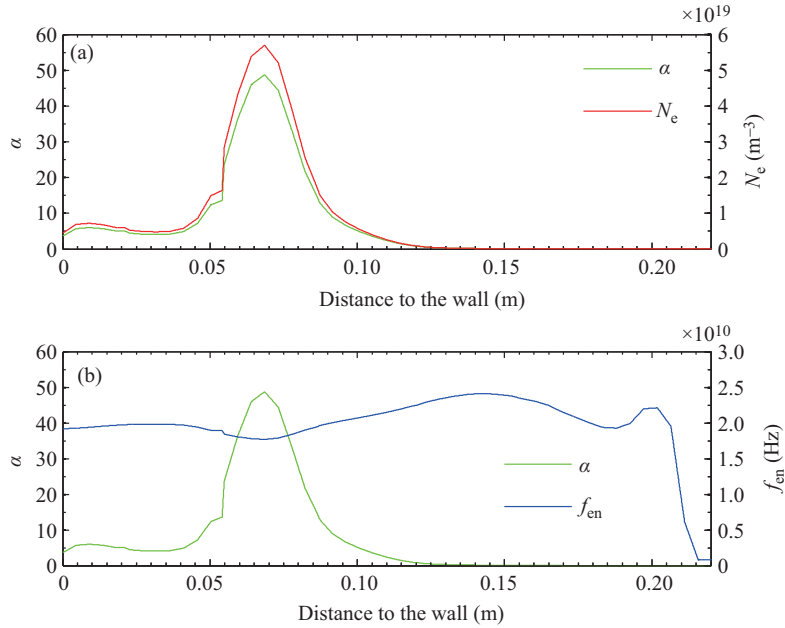
Figure 5   (Color online) The profiles for the attenuation coefficient and the electron density (a) and the electron collision frequency (b).

4   The geographical difference of total signal attenuation over the whole globe

The analysis in Section 3 revealed that the total attenuation of sub-THz signals in hypersonic plasma sheaths is significantly impacted by the atmospheric mass densities. This conclusion was drawn based on the numerical simulations with 11 sets of atmospheric conditions. On the other hand, the global atmospheric conditions is much more complicated. Figure 6 illustrates the global atmospheric mass density and temperature at the altitude of 30 km at 15:15UT on 22 August 1968, which is the time for the RAMC-II experiment [18]. According to Figure 6, both the atmospheric mass density and the temperature vary with latitude and longitude. However, the variation of temperature over the whole globe is ignorable comparing with the temperature itself. Therefore it could be expected that the atmospheric
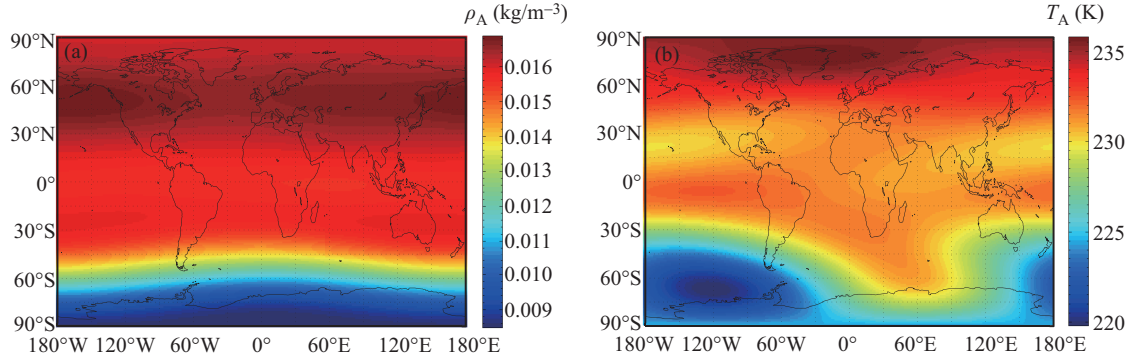
Figure 6 (Color online) The global distributions of atmospheric mass density (a) and temperature (b).

Table 2 The results of curve fitting

	l_{peak}	c_{N_e}	l_{peak1}	c_{c1}	l_{peak2}	c_{c2}	l_{peak3}	c_{c3}
1	0.351	0.01755	0.4344	0.05115	0.4805	0.01166	0.3087	0.1141
2	0.3507	0.01629	0.4348	0.05247	0.4819	0.01061	0.3067	0.1151
3	0.351	0.01723	0.4346	0.05144	0.4807	0.0114	0.3084	0.1138
4	0.3504	0.01663	0.4351	0.0521	0.4819	0.01074	0.3073	0.1175
5	**0.3507**	**0.01638**	**0.4346**	**0.05141**	**0.4815**	**0.01094**	**0.3098**	**0.1121**
6	0.3508	0.0162	0.4348	0.05189	0.4818	0.01074	0.3084	0.115
7	0.3507	0.01656	0.435	0.05195	0.4819	0.01076	0.3078	0.1154
8	0.3508	0.01637	0.4345	0.05197	0.4813	0.01111	0.3076	0.1145
9	0.3507	0.01642	0.4344	0.05218	0.4816	0.01095	0.3064	0.1163
10	0.3507	0.01632	0.4353	0.05152	0.4818	0.01081	0.3094	0.1142
11	0.3508	0.01641	0.4351	0.05202	0.4819	0.01064	0.3082	0.1141

mass density around the vehicle is the dominant factor for the total signal attenuations (Att).

On the other hand, solving the numerical hypersonic fluid model is time consuming. It is impossible to obtain the geographical difference of Att over the whole globe via solving the fluid model. In such a case, a new method, whose efficiency is much higher, is developed based on the analysis in Section 3.

Basically the idea for the new method is approximately estimating the electron density and the electron collision frequency instead of working them out by solving the numerical fluid model. Referring to the characters of the electron density and the collision frequency profiles, the Gaussian functions, which are given below, are selected to approximately describe the two profiles.

$$N_e(l) = N_{e,\text{peak}} \exp\left\{-\left[(l - l_{\text{peak}})/c_{N_e}\right]^2\right\}, \tag{23}$$

$$
\begin{aligned}
f_{\text{en}}(l) = {} & f_{\text{en,peak1}} \exp\left\{-\left[(l - l_{\text{peak1}})/c_{c1}\right]^2\right\} \\
& + f_{\text{en,peak2}} \exp\left\{-\left[(l - l_{\text{peak2}})/c_{c2}\right]^2\right\} \\
& + f_{\text{en,peak3}} \exp\left\{-\left[(l - l_{\text{peak3}})/c_{c3}\right]^2\right\},
\end{aligned}
\tag{24}
$$

where $N_{e,\text{peak}}$ and l_{peak} are the peak value for N_e and the distance from the peak N_e to the antenna, respectively. $f_{\text{en,peak1}}$, $f_{\text{en,peak2}}$, $f_{\text{en,peak3}}$ are the values for the three peaks of f_{en}. l_{peak1}, l_{peak2} and l_{peak3} are the distances from the peaks of f_{en} to the antenna. c_{N_e}, c_{c1}, c_{c2} and c_{c3} are constants, which determine the effective length of signal propagation path. Those coefficients, except the peak values of N_e and f_{en}, are obtained via curve fitting on the previously obtained profiles of N_e and f_{en}. The fitting results are listed in Table 2.

The $N_{e,\text{peak}}$ and the $f_{\text{en,peak}}$ have linear relations with the atmospheric mass density (see Figure 3(c) and (d)). Therefore the two variables could be obtained based on atmospheric mass densities. The data
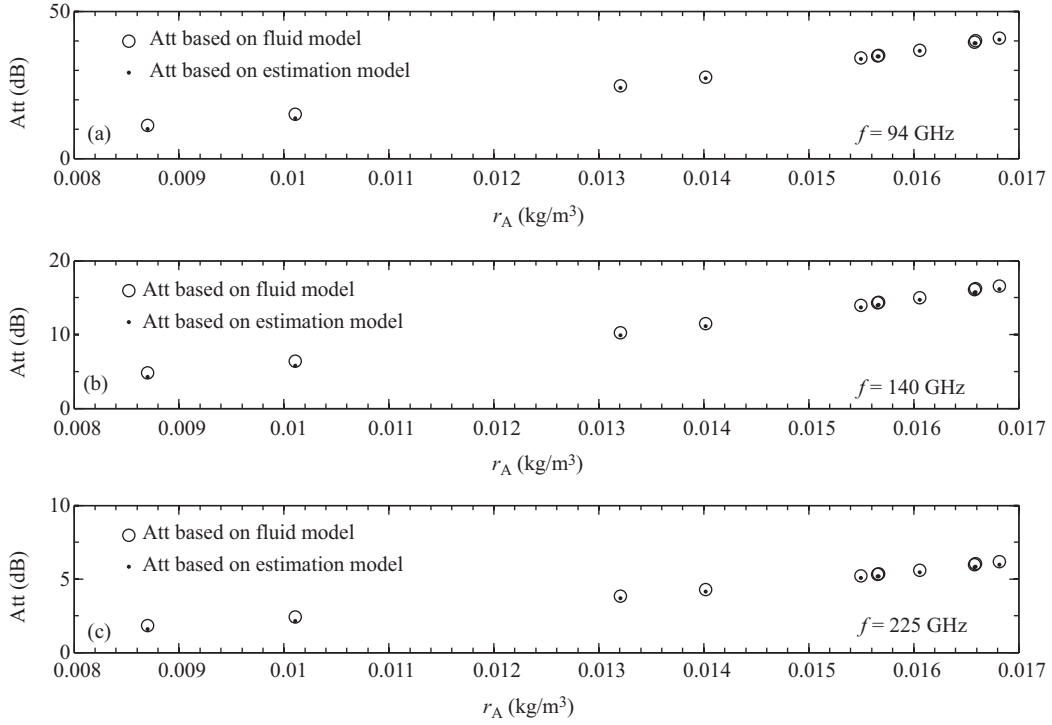
Figure 7 The comparisons between the Att based on the hypersonic fluid model (dots) and the estimation model (circles).

in Table 2 shows that both the distances from the peaks to the antenna and the effective length of signal propagation path fluctuate in very small ranges. In order to test that whether the coefficients obtained via the curve fitting and the peak values for the N_e and f_{en} could be utilized to estimate the Att or not, a set of coefficients, which corresponds to the location at equator and was marked in bold in Table 2, was selected. The electron density and the collision frequency at the other 10 locations were estimated based on (23), (24) and the selected coefficient set. The Att based on the estimation was compared with the Att obtained via solving the numerical fluid model in Figure 7. The results of comparison shows that the estimation method could be utilized to calculate the Att with insignificant errors.

The global distribution of the Att is obtained with the new estimation method. The results are illustrated in Figure 8.

Figure 8 shows that the Att varies with both latitude and longitude. Generally, the Att at northern hemisphere are higher than that at southern hemisphere. The maximum Att appears in the region whose latitudes are between 45°N to 70°N, which covers parts of Canada, Russia and Alaska of the United States. On the other hand, the Att varies with the frequency of carrier wave. For example, if the criteria for the 'blackout' is Att>10 dB, the communication system operating at 94 GHz would suffer from the 'blackout' almost over the whole globe. The system operating at 225 GHz can mitigate the 'blackout' effectively. It should be noticed that the system operating at 140 GHz would suffer from the 'blackout' over the whole globe except the high latitude regions at southern hemisphere.

Since the S/N ratio for the communication varies with the signal strength received by the antenna, the performance of a sub-THz communication system would differ at different geophysical locations. For a sub-THz communication system on hypersonic cruise flights, both the communication quality and the occurrence of communication blackout partly depend on the flight route.

5 Summary and conclusion

In the present study the propagation of sub-THz signals in hypersonic plasma sheath was modeled under different atmospheric conditions. The characters of signal attenuation was analyzed. Based on
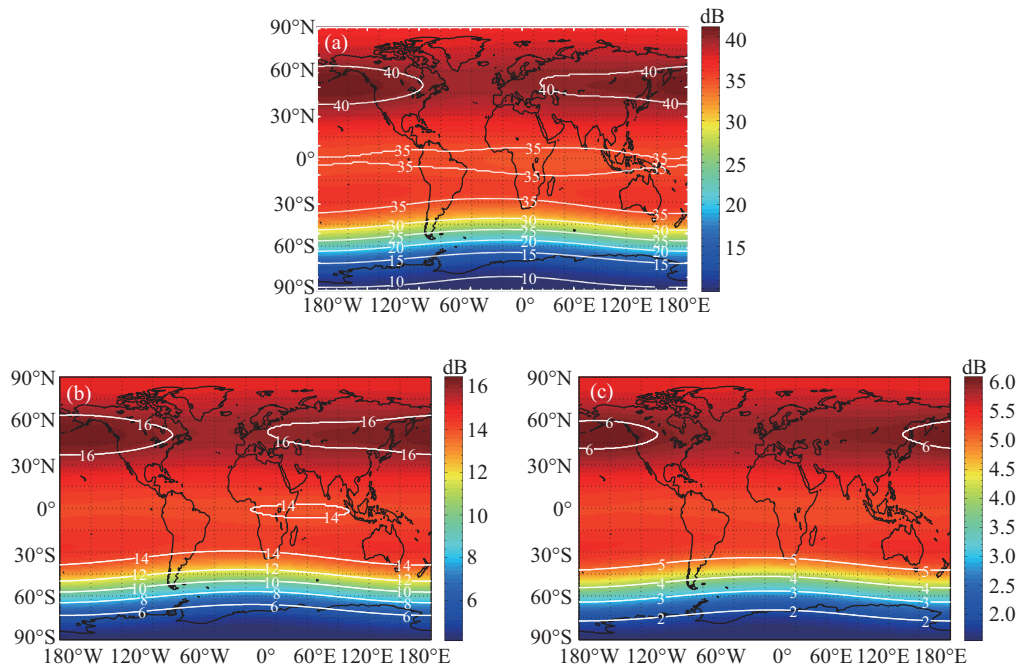
Figure 8   (Color online) The global Att for the signals at (a) 94 GHz, (b) 140 GHz and (c) 225 GHz.

the analysis, a new estimation model for the total attenuation of sub-THz signals in hypersonic plasma sheaths was developed. The geographical difference of the power transmission rate was obtained. The conclusion is drawn below:

(1) The attenuation of sub-THz signals in hypersonic plasma sheaths is impacted by the atmospheric density. The total signal attenuation in hypersonic plasma sheaths increase with the atmospheric mass density around the flight. The impact led by the atmospheric temperature is ignorable.

(2) The peak values of the electron density and the electron collision frequency near the onboard antenna have linear relations with the atmospheric mass density around the vehicle.

(3) The attenuation of sub-THz signals in hypersonic plasma sheaths mainly occurs near where the electrons concentrate.

(4) Due to the geographical difference of atmospheric mass density, the total attenuation of sub-THz signals in hypersonic plasma sheaths varies with the latitude and the longitude of the flight. For a hypersonic cruise flight, the performance of the onboard sub-THz communication system partly depends on the flight route. Generally the total signal attenuation at northern hemisphere are higher than that at southern hemisphere. The maximum total signal attenuation occurs once the flight is in the region between the latitudes of 45°N to 70°N, which covers parts of Canada, Russia and Alaska of the United States.

Conflict of interest   The authors declare that they have no conflict of interest.

Supporting information   The supporting information is available online at info.scichina.com and link. springer.com. The supporting materials are published as submitted, without typesetting or editing. The responsibility for scientific accuracy and content remains entirely with the authors.

References

1   Rybak J P, Churchill R J. Progress in reentry communications. IEEE Trans Aerosp Electron Syst, 1971, 7: 879–894

2 Notake T, Saito T, Tatematsu Y, et al. Development of a novel high power sub-Thz second harmonic gyrotron. Phys Rev Lett, 2009, 103: 225002

3 Koenig S, Lopez-Diaz D, Antes J, et al. Wireless sub-Thz communication system with high data rate. Nature Photon, 2013, 7: 977–981

4 Zheng L, Zhao Q, Liu S, et al. Theoretical and experimental studies of 35 GHz and 96 GHz electromagnetic wave propagation in plasma. Prog Electromagn Res M, 2012, 24: 179–192

5 Zheng L, Zhao Q, Liu S Z, et al. Theoretical and experimental studies of terahertz wave propagation in unmagnetized plasma. J Infrared Millim Terahertz Waves, 2014, 35: 187–197

6 Li J, Pi Y, Yang X. A conception on the terahertz communication system for plasma sheath penetration. Wirel Commun Mobile Comput, 2015, 14: 1252–1258

7 Tian Y, Han Y P, Ling Y J, et al. Propagation of terahertz electromagnetic wave in plasma with inhomogeneous collision frequency. Phys Plasmas, 2014, 21: 1768–1775

8 Yuan C X, Zhou Z X, Zhang J W, et al. FDTD analysis of terahertz wave propagation in a high-temperature unmagnetized plasma slab. IEEE Trans Plasma Sci, 2011, 39: 1577–1584

9 Chen J M, Yuan K, Shen L F, et al. Studies of terahertz wave propagation in realistic reentry plasma sheath. Prog Electromagn Res, 2016, 157: 21–29

10 Meyer J W. System and Method for Reducing Plasma Induced Communication Disruption Utilizing Electrophilic Injectant and Sharp Reentry Vehicle Nose Shaping. US Patent, 2007, US7237752

11 Jung M, Kihara H, Abe K I, et al. Numerical analysis on the effect of angle of attack on evaluating radio-frequency blackout in atmospheric reentry. J Korean Phys Soc, 2016, 68: 1295–1306

12 Yuan K, Yao M, Shen L F, et al. Studies on the effect of angle of attack on the transmission of terahertz waves in reentry plasma sheaths. Prog Electromagn Res M, 2017, 54: 175–182

13 Starkey R P. Hypersonic vehicle telemetry blackout analysis. J Spacecraft Rockets, 2015, 52: 426–438

14 Kundrapu M, Loverich J, Beckwith K, et al. Modeling radio communication blackout and blackout mitigation in hypersonic vehicles. J Spacecraft Rockets, 2015, 52: 853–862

15 Gupta R N, Yos J M, Thompson R A, et al. A review of reaction rates and thermodynamic and transport properties for an 11-species air model for chemical and thermal nonequilibrium calculations to 30000 K. Nasa Sti/recon Tech Rep N, 1990, 89: 32–34

16 Liebe H J. Atmospheric ELF window transparencies near 35, 90, 140 and 220 GHz. IEEE Trans Antenn Propag, 1983, 31: 127–135

17 Bachynski M, Johnston T, Shkarofsky I. Electromagnetic properties of high-temperature air. Proc IRE, 1960, 48: 347–356

18 Jones W L, Cross A E. Electrostatic-Probe Measurements of Plasma Parameters for two Reentry Flight Experiments at 25000 Feet per Second. Technical Report NASA TN D-6617. 1972